Chemical Engineering Journal 158 (2010) 188–199

Contents lists available at ScienceDirect

Chemical Engineering Journal

journal homepage: www.elsevier.com/locate/cej

Moringa oleifera—A solid phase extractant for the removal of copper, nickel and zinc from aqueous solutions

M. Helen Kalavathy, Lima Rose Miranda*

Department of Chemical Engineering, A.C. College of Technology, Anna University, Chennai 600 025, India

ARTICLE INFO

Article history:
Received 22 July 2009
Received in revised form
15 December 2009
Accepted 21 December 2009

Keywords:
Moringa oleifera
SEM
FT IR
Heavy metals
Adsorption isotherms
Adsorption mechanism
Desorption

ABSTRACT

Moringa oleifera (MO) wood, a solid waste was used for the preparation of activated carbon (ACMO) for the removal of copper, nickel and zinc from synthetic wastewater. Effects of various operating variables namely solution pH, contact time, carbon dose, adsorbate concentration and temperature on the removal of metal ions have been studied. Thermodynamic parameters such as free energy change, enthalpy change and entropy change were calculated. The optimum pH for the adsorption for all the above mentioned metals was found to be 6. The adsorption process was found to be endothermic for Cu and exothermic for Ni and Zn. The Langmuir, Freundlich, Temkin and Dubinin Radushkevich isotherm models were used to analyze the equilibrium data at different temperatures. The data were also fitted to kinetic models such as pseudo-first-order and pseudo-second-order model. Kinetic studies showed that the adsorption followed a pseudo-second-order model. The intra-particle diffusion rate constants and effective diffusion coefficient for different temperatures were evaluated and discussed. Adsorption occurs both by film diffusion and particle diffusion mechanism. The ACMO could be regenerated using 0.1 M H_2SO_4, with up to 98% recovery for all the three metals.

1. Introduction

Among the natural substances that man concentrates in his immediate environment, metals are the most ubiquitous. These inorganic pollutants largely originate from industrial wastes. Self purification is also hindered by the presence of heavy metal ions in water. Metals can be neither degraded nor metabolized; these are an example of ultimate persistence [1,2]. Among the heavy metals, arsenic, copper, cadmium, lead, mercury, nickel and zinc are the ones that have most severely affected the environment. It is well established that the presence of heavy metals in the environment, even in moderate concentration is responsible for producing a variety of illnesses related with the risk of dermal damage, respiratory problems and several kinds of cancer, as accurately reviewed in a recent papers [3–6]. Mining, electroplating, metal processing, textile and battery manufacturing industry are the main sources of heavy metal ion contamination. The World Health Organization (WHO) recommends a maximum acceptable concentration of copper, nickel and zinc in drinking water of 2, 0.02 and 3 mg L^{-1} respectively [7].

Various treatment technologies have been developed for the removal of these metals from wastewater, such as precipitation, oxidation/reduction, coagulation–flocculation, electro coagulation, cementation, membrane separation, membrane filtration, solvent extraction, ion-exchange, adsorption and biosorption, etc. [8,9] depending on the concentration. Adsorption methods do offer the most direct method of producing highest quality treated water. However, the other methods have significant disadvantages such as incomplete metal removal, particularly at low concentrations and high capital investment as well as creating sludge disposal problem [10]. Adsorption phenomenon is commonly used due to its relatively high efficiency, harmlessness to the environment and ease in operation. A number of workers have used different adsorbent systems, developed from various industrial waste materials, for the removal of heavy metals [11,12]. Some of these low-cost sorbents include peat, bark, lignin, agricultural wastes, fly ash, and clay minerals [13].

Biological techniques for metal removal have also been reported in literature. These include application of sequencing batch reactor (SBR) system for removing Zn^{2+} and Cu^{2+} [14] and the application of pre-treated biomass of Australian marine algae in biosorption of lead(II) and copper(II) from aqueous solutions [15]. There still exists a need to develop a low-cost and efficient adsorbent for the removal of heavy metals from wastewater.

Adsorption using activated carbon has still been found to be economically appealing for the removal of toxic metals from wastewater by choosing adsorbents under optimum operating conditions. Activated carbon is a unique and effective agent for purification, isolation and recovery of trace metal. During the last

* Corresponding author. Tel.: +91 9444827462; fax: +91 4445500224.
E-mail addresses: helenkalavathy@gmail.com (M. Helen Kalavathy), limamiranda2007@gmail.com (L.R. Miranda).

1385-8947/$ – see front matter © 2010 Elsevier B.V. All rights reserved.
doi:10.1016/j.cej.2009.12.039

Nomenclature

A	Temkin constants relating to sorption potential ($L\,g^{-1}$)
b	Langmuir constant representing adsorption intensity ($L\,mg^{-1}$)
B	Temkin constants relating to heat of adsorption
C_o	Initial concentration of metal ion in solution ($mg\,L^{-1}$)
C_e	Equilibrium concentration of metal ion in solution ($mg\,L^{-1}$)
C_t	Concentration of metal ion in solution at any time t ($mg\,L^{-1}$)
C_{Ae}	Equilibrium concentration of metal ion in the solution ($mg\,L^{-1}$)
C_{Be}	Equilibrium concentration of metal ion on the adsorbent ($mg\,L^{-1}$)
D_e	Effective diffusion coefficient ($m^2\,s^{-1}$)
E_s	Adsorption energy ($kJ\,mol^{-1}$)
$F(t)$	Fractional attainment of equilibrium at time t
K	D–R constant related to mean free energy of adsorption
K_c	Equilibrium constant
K_1	Pseudo-first-order rate constant (min^{-1})
K_2	Pseudo-second-order rate constant ($g\,mg^{-1}\,min^{-1}$)
K_f	Multilayer adsorption capacity ($mg\,g^{-1}$)
K_{id}	Initial rate of intra-particle diffusion ($mg\,(g\,min^{0.5})^{-1}$)
M	Mass of the adsorbent (g)
n	Adsorption intensity ($g\,L^{-1}$)
q_e	Adsorption capacity at equilibrium ($mg\,g^{-1}$)
q_m	Theoretical saturation capacity ($mg\,g^{-1}$)
q_t	Adsorption capacity at any time t ($mg\,g^{-1}$)
R	Universal gas constant ($kJ\,kg^{-1}\,mol^{-1}\,K^{-1}$)
R^2	Correlation coefficient
R_a	Radius of spherical adsorbent particles (m)
t	Contact time (min)
T	Temperature (K)
V	Volume of adsorbate solution (L)
X_m	Monomolecular adsorption capacity ($mg\,g^{-1}$)

Greek letters

ε	Polanyi potential
ΔG°	Standard Gibbs free energy change
ΔH°	Standard enthalpy change
ΔS°	Standard entropy change

three decades, the treatment with activated carbon has become an important unit process for separation and purification in a wide range of industries. There are two methods of preparing activated carbon: physical activation and chemical activation. The advantage of chemical activation over physical activation is that it can be performed in a single step and at relatively low temperatures (usually $\leq$773 K for activation of wood by H_3PO_4 [16] and between 873 and 973 K for activation of lignocellulosic materials impregnated with $ZnCl_2$ [17]). The chemical agent promotes the formation of cross-links, leading to the formation of a rigid matrix that is further less prone to volatile loss and volume contraction upon heating to high temperatures [18,19]. However, phosphoric acid is preferred because of the problems of corrosion, inefficient chemical recovery, and environmental disadvantages associated with zinc chloride. It is well known that activation with phosphoric acid develops micro porosity when using cellulosic and lignocellulosic precursors in the manufacture of activated carbon. Chemical activation is carried out in two steps, in the first one the precursor is impregnated with phosphoric acid and in the second the heat treatment influences the carbonization process, generating the porosity, which becomes accessible when phosphoric acid is removed by washing. Consequently, the modification of chemical-precursor ratio permits the adjustment of porosity in the activated carbon.

A number of works have been carried out using Moirnga oleifera (MO) as an adsorbent for the removal of heavy metals from aqueous solutions [20–24]. However, no attempt has been made to prepare activated carbon from MO wood.

In the present work, an attempt has been made to develop an inexpensive adsorbent system for the removal of copper, nickel and zinc from aqueous solution using *Moringa oleifera* wood. MO wood has no utility and therefore a cause of environmental degradation [23]. Moreover, the tree is normally cut back annually to less than 1 m and allowed to regrow, so that pods and leaves remain within arm's reach. The carbon from MO wood has extensive surface area, which is a suitable attribute for metal adsorption. Therefore, MO wood is employed for the preparation of activated carbon and using the same for the adsorption of above mentioned metals. The adsorption capacity of copper, nickel and zinc were examined by varying experimental conditions, viz. solution pH, contact time, adsorbent dose, ionic strength, and temperature. The experimental data were correlated to different kinetic and adsorption isotherm models and the corresponding parameters were determined. These parameters are considered fundamental for further studies involving the scale-up of the process for continuous studies. Also these results could be useful in understanding and developing a process for removing these metals from wastewaters.

2. Materials and methods

2.1. Preparation of the adsorbent

Moringa oleifera wood was collected from different regions in and around Chennai, the outer pericarp was removed and they were cut into small pieces. Soluble and coloured components were removed from the wood by washing with boiling water. This was repeated until the water was virtually colourless. The wood chips were then washed with distilled water and dried in a hot air oven at 383 K till it reaches constant weight. After this they were ground and sieved to particle size of 1 mm.

The sample was then mixed with the phosphoric acid at an impregnation ratio of 1:2 (weight of MO: weight of phosphoric acid) and soaked for 24 h so that the reagents were fully adsorbed onto the raw material. The mixture was dried at 383 K for 1.5 h and then transferred to a sealed ceramic container. The dried mixture was activated in a muffle furnace at 673 K for a period of 1 h. The carbons (ACMO) thus produced were then repetitively washed with distilled water to recover all the acid and then with 1% $NaHCO_3$ solution to remove the residual acid [25]. The activated carbon was powdered, sieved and stored in sealed containers. The fraction which passed through 200 mesh screen was used for all the experiments.

2.2. Characterization of adsorbents

The ACMO was characterized by finding out its pH_{PZC} [26], iodine number, methylene blue number, methyl violet number and surface area. These numbers are determined as per the standard procedures [27]. The proximate analysis of the raw material and the properties of activated carbon prepared are given in Table 1.

In order to observe the surface morphology of the adsorbent, scanning electron microscopic (SEM) analysis was employed in

Table 1
Proximate analysis of MO and the properties of ACMO.

Characteristics of the adsorbent	Characteristics values
Moisture (%)	9.51
Volatile matter (%)	27.32
Carbon (%)	55.58
Ash (%)	7.59
Particle size (mm)	0.074
pH_{PZC}	6.25
BET surface area ($m^2\,g^{-1}$)	787.34
Pore volume ($cm^3\,g^{-1}$)	0.76
Iodine number ($mg\,g^{-1}$)	1135.26
Methylene blue number ($mg\,g^{-1}$)	145
Methyl violet number ($mg\,g^{-1}$)	140
Bulk density ($g\,cm^{-3}$)	0.38
Yield (%)	58.7

this study. SEM images were recorded using JEOL JSM-6360 field emission SEM.

The surface functional groups of adsorbents were identified using Fourier transform infrared spectrophotometer (FT IR). Fourier transform infrared spectra were obtained using a spectroscope (Tensor 29, Bruker) at resolution 1 cm^{-1}. Pressed potassium bromide (KBr) pellets at a sample/KBr weight ratio of 1:100 were scanned and recorded between 4000 and 400 cm^{-1}.

2.3. Synthetic wastewater preparation

Synthetic wastewater solutions were prepared by dissolving analytical grade $CuSO_4{\cdot}5H_2O$, $NiSO_4{\cdot}7H_2O$ and $ZnSO_4{\cdot}7H_2O$ in distilled water to obtain a stock solution of 1000 mg L^{-1} metal solution. The working solution was diluted to the required concentration for experiments. The pH of the solutions was adjusted using sulphuric acid and sodium hydroxide. All the other chemicals used for the analysis of metal ions were of analytical grade.

2.4. Batch adsorption studies

A series of Erlenmeyer flasks of 250 mL capacity containing desired amount of metal ion solutions of known concentrations and ACMO were agitated in a temperature controlled shaker (Orbital, Scigenics) at 180 rpm. The effect of contact time (0–240 min), initial metal ion concentration (10–50 mg L^{-1}), solution pH (2.0–10), carbon dose (0.05–0.7 g (100 mL)$^{-1}$), and temperature (293–323 K) were studied. The pH of the solutions was adjusted using H_2SO_4 or NaOH. Samples were taken at prescribed time intervals; the solutions were centrifuged and the supernatant was analyzed for metal ion concentration using UV spectrophotometer (Shimadzu Model UV-2100S).

The amount of metal ions adsorbed at any time t, was calculated using the equation

$$q_1 = \frac{(C_o - C_t)V}{M} \quad (1)$$

where V is the adsorbate volume (L), M the amount of ACMO (g), and C_o and C_t (mg L^{-1}) are the initial concentration of metal ion and concentration of metal ion at any time t, respectively.

2.5. Metal ion analysis

The concentrations of the copper at different time intervals were analyzed in a spectrophotometer by forming a complex with sodium diethyl dithiocarbamate at a wavelength of 435 nm. Similarly the concentration of nickel and zinc were determined by forming complex with dimethyl glyoxime and zincon and analyzing at a wavelength of 470 and 520 nm respectively [28,29].

2.6. Batch desorption studies

For desorption studies analytical grade HCl, H_2SO_4, HNO_3, Na_2CO_3, EDTA, $NaHCO_3$, NH_4Cl, and CH_3COOH were used. For batch desorption experiments, a series of 250 mL Erlenmeyer flasks containing 100 mL desorption solution of known concentration was contacted with metal loaded ACMO (0.2 g) at 303 K. The mixtures were agitated in an orbital shaker at 180 rpm for 30 min. The ACMO was removed, centrifuged and the supernatant was analyzed for metal concentration released into the solution.

3. Results and discussion

3.1. Characterization of adsorbents

The surface morphology of the AC was studied with scanning electron microscopy. The information on the chemical structure of the adsorbent material was provided by FT IR.

3.1.1. Scanning electron micrographs

The SEM images clearly reveal the surface texture and morphology of the adsorbent (Fig. 1a,b). The surface morphology of raw *Moringa oleifera* (RMO) is different from that of ACMO. The RMO has more irregular surface and no pores are seen, but after carbonizing and activating, ACMO are more porous and the surface becomes homogenous when compared to RMO and therefore has a larger specific surface area. The micrographs of ACMO reveal clearly the presence of cylindrical structures, with different diameters. This surface characteristic would result in the higher adsorption capacity.

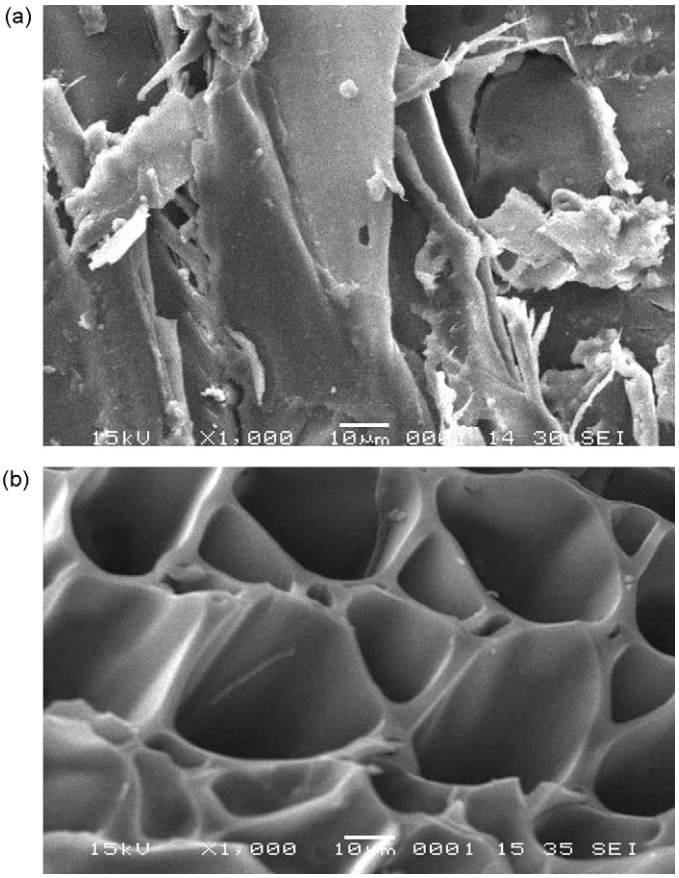

Fig. 1. a: SEM of raw MO. b: SEM of ACMO.

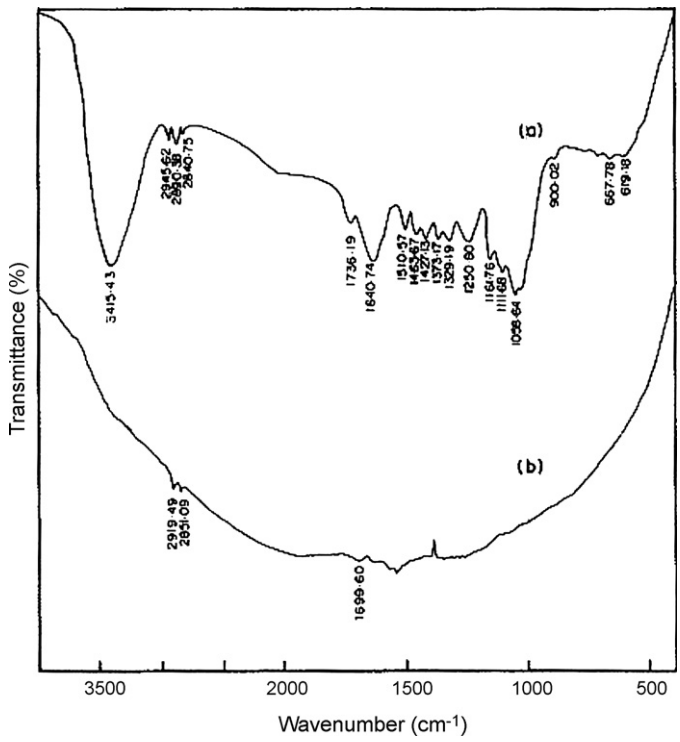

Fig. 2. FT IR spectra of (a) raw MO and (b) ACMO.

3.1.2. Fourier transform infrared spectroscopy

The IR spectrum of RMO was compared with that of ACMO. Fig. 2a,b shows the spectra of RMO and ACMO. In Fig. 2a, the broad band around 3415 cm^{-1} was attributed to the surface hydroxyl groups and chemisorbed water. The bands between 2945 and 2840 cm^{-1} were assigned to stretching vibration of C–H alkane group. The bands between 1736 and 1640 cm^{-1} were attributed to strong C=O ketonic and aldehyde group. Small peaks observed at 1510 cm^{-1} and 1468–1300 cm^{-1} can be assigned to CH_3–C alkanes and COO^- carboxylate groups respectively. At around 1250 cm^{-1} the band can be assigned to COOH group. The bands below 1200 cm^{-1} can be considered as finger print regions.

No peaks are observed corresponding to any functional group for ACMO (Fig. 2b). The disappearance of the above mentioned groups may be due to hydrolysis effect of H_3PO_4, resulting in the decomposition of these groups and subsequent release of their by-products as volatile matter. This proves that there is no functional group on the surface of the ACMO and it is only elemental carbon. Therefore, the removal of Cu, Ni and Zn from aqueous solution is not due to complex formation phenomenon with surface functional group and it is only adsorption which is surface phenomena.

3.2. Effect of operating variables

3.2.1. Effect of contact time

Fig. 3 shows the percentage removal of Cu, Ni and Zn as a function of time. The dependence of adsorption of metal ions on ACMO with contact time was carried out for initial metal ion concentration of 30 mg L^{-1}, fixed carbon dosage of 0.2 g (100 mL)$^{-1}$ at 303 K and natural pH. The percentage removal was found to increase with increasing contact time and attained maximum value at 4 h for copper, 1 h for nickel and 3 h for zinc. The results showed that a rapid increase in Cu and Zn adsorption occurred within 10 min with more than 50% of total adsorption. In the case of nickel, about 80% of adsorption was completed within 2 min. There was no significant change in equilibrium concentration after 4, 1 and 3 h for Cu, Ni and Zn removal. But for the sake of comparison all other experiments were carried out for 4 h for all the above mentioned metals.

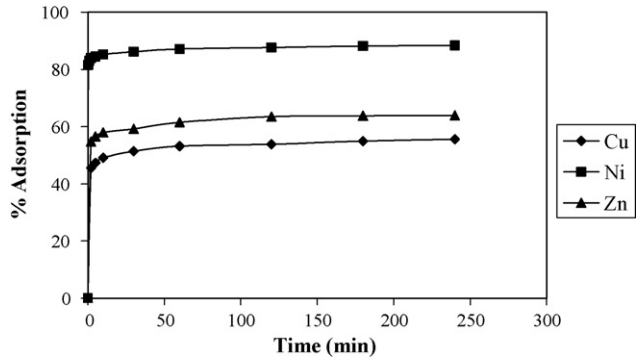

Fig. 3. Effect of contact time on % adsorption of Cu, Ni and Zn, and comparison between Cu, Ni and Zn. Initial metal ion concentration 30 mg L^{-1}, carbon dosage 0.2 g (100 mL)$^{-1}$, temperature 303 K, natural pH.

Fig. 3 also shows the comparison between copper, nickel and zinc removal. It can be observed that the percentage removal is maximum in the case of Ni to an extent of 88.36% followed by Zn (63.90%) and Cu showing the least adsorption capacity of 55.60%. All the values are given at equilibrium time and conditions as stated earlier.

3.2.2. Effect of pH

Effect of initial solution pH on adsorption was determined by shaking 0.2 g of ACMO with 100 mL of solution containing initial metal ion concentration of 30 mg L^{-1} at various pH values ranging from 2 to 10. Fig. 4 shows adsorption capacity of ACMO for the adsorption of Cu, Ni and Zn as a function of pH. In all the three cases the adsorption is very low in the pH range 2–4. On increasing the pH above 6, the adsorption capacity rapidly increases. This phenomenon can be explained by the surface charge of the ACMO and the H^+ ions present in the solution. At low pH the cations compete with the H^+ ions in the solution for the active sites and therefore lower adsorption. The surface charge of the ACMO is a strong function of the pH. The pH_{PZC} of ACMO is 6.25. Therefore at pH value above pH_{PZC}, surface of the ACMO has a higher negative charge which results in higher attraction of metal ions (cations) [30]. At pH value below pH_{PZC}, the surface charge of ACMO is positive and hence the adsorption capacity decreases. However, in our work, an optimum initial pH was chosen to be 6 because precipitation of metal hydroxide was observed at pH greater than 6. These data are in agreement with the results obtained in our earlier work [25].

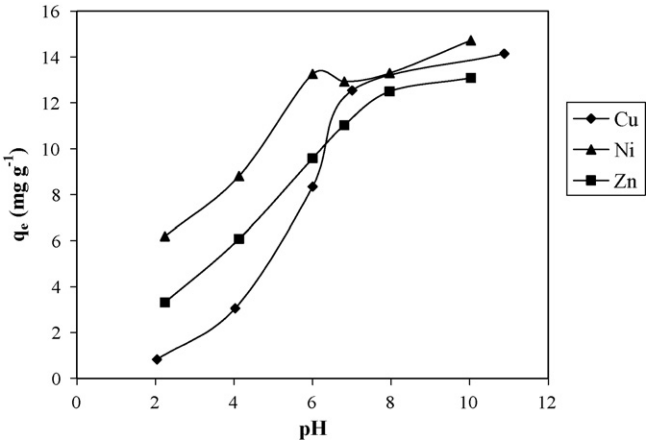

Fig. 4. Effect of pH on adsorption capacity of ACMO. Initial metal ion concentration 30 mg L^{-1}, carbon dosage 0.2 g (100 mL)$^{-1}$, temperature 303 K, contact time 4 h.

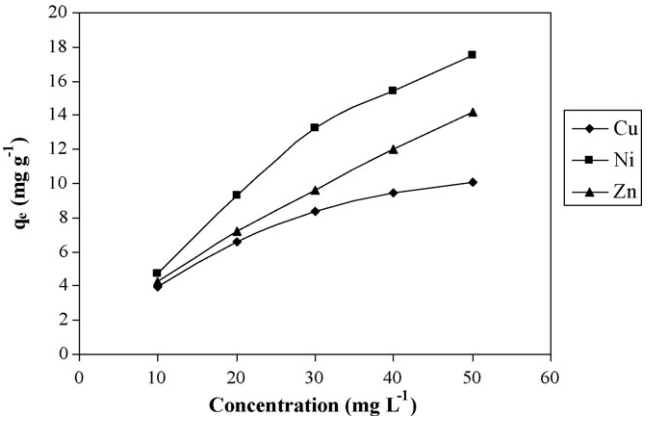

Fig. 5. Effect of initial metal ion concentration on adsorption capacity of ACMO, carbon dosage 0.2 g (100 mL)$^{-1}$, temperature 303 K, contact time 4 h, pH 6.

3.2.3. Effect of initial metal ion concentration

The effect of initial metal ion concentration on adsorption capacity of ACMO was carried out at a carbon dosage of 0.2 g (100 mL)$^{-1}$, pH 6, contact time 4 h, temperature 303 K for different initial metal ion concentration (10–50 mg L^{-1}) and is shown in Fig. 5. As shown, the amount of metal uptake per unit weight of the adsorbent increases with increasing initial metal ion concentration showing the maximum adsorption capacity of 10.08 mg g^{-1}, 17.48 mg g^{-1} and 14.16 mg g^{-1} for Cu, Ni and Zn respectively. This is because at higher initial concentrations, the ratio of initial number of moles of metal ions to the available adsorption surface area is high. This may be attributed to an increase in the driving force of the concentration gradient with the increase in the initial metal concentration [31].

3.2.4. Effect of carbon dosage

The effect of carbon dosage for the removal of Cu, Ni and Zn on adsorption capacity were studied by varying the amount of carbon from 0.05 to 0.7 g (100 mL)$^{-1}$, while keeping other parameters (pH 6, agitation speed 180 rpm, temperature 303 K and contact time 4 h) constant and is shown in Fig. 6. Adsorption capacity decreases from 17.54 to 3.95 mg g^{-1} for copper removal, from 38.75 to 6.5 mg g^{-1} for nickel removal and from 12.32 to 4.13 mg g^{-1} for zinc removal when carbon dosage increases from 0.05 to 0.7 g (100 mL)$^{-1}$. In all the three cases, the amount of metal ions adsorbed per unit weight of adsorbent (q_e) decreases with increase in carbon dose [32]. This is due to the fact that at higher carbon dose, the solution metal ion concentration drops to a lower value and the system reaches equilibrium at lower values of 'q_e' indicating the adsorption sites remain unsaturated. This is due to the fact that the actual number of active sites per gram of adsorbent does not increase proportionately and hence there is a regular decrease in adsorption capacity.

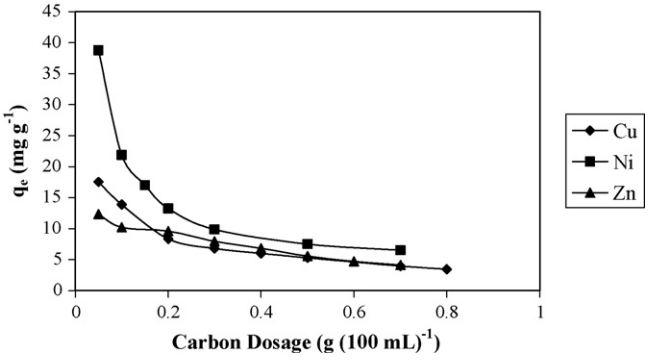

Fig. 6. Effect of carbon dosage on adsorption capacity of ACMO, initial metal ion concentration 30 mg L^{-1}, temperature 303 K, contact time 4 h, pH 6.

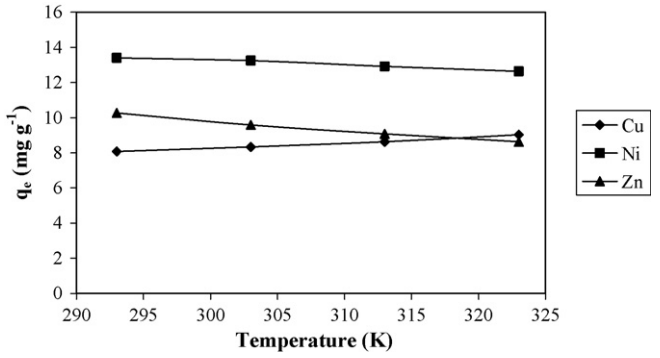

Fig. 7. Effect of temperature on adsorption capacity of ACMO, initial metal ion concentration 30 mg L^{-1}, carbon dosage 0.2 g (100 mL)$^{-1}$, contact time 4 h, pH 6.

3.2.5. Effect of temperature

To study the thermodynamic properties of adsorption, the studies were carried out at 293, 303, 313 and 323 K.

The adsorption of Cu, Ni and Zn onto ACMO as a function of temperature is illustrated in Fig. 7 which shows that the adsorption capacity of nickel and zinc decreased from 13.4 to 12.63 mg g^{-1} and 10.271 to 8.635 mg g^{-1} with temperature indicating that the process is exothermic. But for Cu, the adsorption capacity increased from 8.077 to 9.027 mg g^{-1} with increase in temperature. This increase in adsorption capacity is due to the chemical interaction between metal ion and ACMO, creation of active surface centers or by an enhanced rate of intra-particle diffusion of Cu ions into the pores of the adsorbent at higher temperatures [33]. This indicates that the adsorption of Cu onto ACMO is an endothermic process.

The adsorption equilibrium data obtained for different temperatures were used to calculate the important thermodynamic properties such as standard Gibbs free energy (ΔG°), standard enthalpy change (ΔH°) and standard entropy change (ΔS°) [34]. The standard Gibbs free energy was evaluated by

$$\Delta G^\circ = -RT \ln K_c \quad (2)$$

The equilibrium constant K_c was calculated using the relationship

$$K_c = \left[\frac{C_{Be}}{C_{Ae}}\right] \quad (3)$$

where C_{Be} and C_{Ae} are the equilibrium concentration of metal ions on the adsorbent and solution (mg L^{-1}), respectively. The standard enthalpy (ΔH°) and entropy (ΔS°) of adsorption were determined from the Van't Hoff equation,

$$\ln K_c = \left[\frac{\Delta S^\circ}{R} - \frac{\Delta H^\circ}{RT}\right] \quad (4)$$

where ΔH° and ΔS° were obtained from the slope and intercept of the Van't Hoff's plot of $\ln K_c$ versus $1/T$. The thermodynamic parameters for copper, nickel and zinc at different temperatures are listed in Table 2. The negative values of ΔG° reveal that the adsorption is feasible and spontaneous. The values become more negative with increase in temperature for Cu, but in the case of Ni and Zn, ΔG° become less negative indicating less driving force and hence resulting in lesser adsorption capacity at higher temperatures. The typical range of bonding energy for an ion-exchange mechanism is 1.91–3.82 kcal mol^{-1} (7.9948–15.9897 kJ mol^{-1}) [35]. It is to be noted that ΔG° values up to 15.9897 kJ mol^{-1} are consistent with electrostatic interaction between adsorption sites and the metal ion (physical adsorption). The values of ΔG° obtained in this work, ranges from −0.3753 to −1.109 kJ mol^{-1} for Cu, −5.18 to

Table 2
Thermodynamic parameters for the adsorption of copper, nickel and zinc on ACMO.

T (K)	Copper			Nickel			Zinc		
	ΔG° (kJ mol^{-1})	ΔH° (kJ mol^{-1})	ΔS° (kJ mol^{-1} K^{-1})	ΔG° (kJ mol^{-1})	ΔH° (kJ mol^{-1})	ΔS° (kJ mol^{-1} K^{-1})	ΔG° (kJ mol^{-1})	ΔH° (kJ mol^{-1})	ΔS° (kJ mol^{-1} K^{-1})
293	−0.3753	6.7080	0.0241	−5.1784	−12.2257	−0.02384	−1.8892	−12.2715	−0.0356
303	−0.5671			−5.1057			−1.4383		
313	−0.7909			−4.7569			−1.1110		
323	−1.1090			−4.4915			−0.8194		

−4.49 kJ mol^{-1} for Ni, and −1.89 to −0.8194 kJ mol^{-1} for Zn indicating that electrostatic attraction is the major mechanism responsible for the metal ion adsorption process. The positive values of ΔH° indicate that the adsorption process is endothermic in nature and the positive ΔS suggests the increased randomness at solid liquid interface during the adsorption of Cu on ACMO. During the adsorption of Cu, the adsorbed solvent molecules, which are displaced by the metal ions, gain more translational entropy than is lost by the adsorbate ions, thus allowing for the prevalence of randomness in the system [36]. The values of ΔH° are negative for Ni and Zn adsorption, indicating that the adsorption process is exothermic in nature. The negative values of ΔS° indicate greater order of reaction during adsorption of Ni and Zn on the ACMO surface.

3.3. Adsorption isotherms

Langmuir, Freundlich, Temkin and Dubinin–Radushkevich isotherm models were used to describe the equilibrium data.

3.3.1. Langmuir model

According to Langmuir, the uptake occurs on a homogenous surface by monolayer adsorption with constant heat of adsorption for all sites and without interaction between adsorbed molecules. The Langmuir model [37] can be given as

$$q_e = \left[\frac{XmbC_e}{1 + bC_e}\right] \tag{5}$$

where C_e is the equilibrium concentration of metal ion in the solution (mg L^{-1}), q_e is the amount of the metal ion adsorbed at equilibrium (mg g^{-1}), X_m is the amount of metal ion required to form a monolayer, i.e., adsorption capacity of the adsorbent (mg g^{-1}), and b(L mg^{-1}) is the equilibrium constant related to free energy or net enthalpy of adsorption ($b \alpha e^{-\Delta H/RT}$). The above equation can be linearized and a plot of C_e/q_e versus C_e should be a straight line with slope $1/X_m$ and intercept $1/X_m b$ when adsorption follows the Langmuir model.

3.3.2. Freundlich model

The Freundlich expression is an empirical equation based on adsorption on a heterogeneous surface. The Freundlich model does not indicate a finite sorbent uptake capacity and can only be applied in the low to intermediate concentration range. The general Freundlich equation is as follows [38]:

$$q_e = K_f(C_e)^{1/n} \tag{6}$$

where K_f (mg g^{-1}) and $1/n$ (L g^{-1}) are Freundlich isotherm constants relating multilayer adsorption capacity and adsorption intensity. The above equation is linearized and a plot of log q_e versus log C_e will give a straight line of slope $1/n$ and intercept K_f.

3.3.3. Temkin model

Temkin and Pyzhev [39] considered the effect of indirect interaction between the metal ions and adsorbent on adsorption isotherms. Because of these interactions, the heat of adsorption of all the molecules in the layer would decrease linearly with surface coverage. The Temkin equation is given as,

$$q_e = \frac{RT}{B} \ln(AC_e) \tag{7}$$

where A (L g^{-1}) and B are Temkin constants relating to adsorption potential and heat of adsorption.

It can be linearized as follows.

$$q_e = \frac{RT}{B} \ln(A) + \frac{RT}{B} \ln(C_e) \tag{8}$$

A plot of q_e versus ln C_e gives the values of Temkin constants A and B.

3.3.4. Dubinin–Radushkevich model

The Dubinin–Radushkevich (D–R) isotherm [40] is more general because it does not assume a homogeneous surface or constant adsorption potential.

The D–R equation is given by,

$$q_e = q_m \exp(-K\varepsilon^2) \tag{9}$$

Its linear form can be represented as

$$\ln q_e = \ln q_m - K\varepsilon^2, \tag{10}$$

where q_e is the amount of the metal ion adsorbed at equilibrium, K is a constant related to the mean free energy of adsorption, q_m is the theoretical saturation capacity, ε is the Polanyi potential, equal to $RT \ln(1 + (1/C_e))$. The values of q_m and K were determined by plotting ln q_e versus ε^2.

The values of sorption energy (E_s) (kJ mol^{-1}) can be calculated from the equation,

$$E_s = \frac{1}{\sqrt{2K}} \tag{11}$$

If the magnitude of E_s is between 8 and 16 kJ mol^{-1}, the adsorption process proceeds by ion-exchange or chemisorption [35,41], while for values of E_s < 8 kJ mol^{-1}, the adsorption process is of a physical nature [42].

The isotherm constants and corresponding correlation coefficients for the adsorption of Cu, Ni and Zn at different temperatures are presented in Table 3. The correlation coefficients demonstrate that Langmuir, Freundlich and Temkin models adequately fitted the data for Cu adsorption. However, R^2 values are higher in the Langmuir model for Ni and Freundlich model for Zn adsorption when compared to other models. The Temkin isotherm shows a higher correlation coefficient for all the metals, which may be due to the linear dependence of heat of adsorption at low or medium coverages. This linearity may be due to repulsion between adsorbate species or to intrinsic surface heterogeneity. The analysis of monolayer adsorption capacity, X_m with temperature in Table 3 indicates that the adsorption is endothermic process for Cu and exothermic for Ni and Zn. The values of n in Freundlich isotherm are in the range 2.17–2.92, which indicates favorable adsorption process [43]. The values of sorption energy (E_s) for Cu, Ni and Zn show that the interaction between metal ions and the adsorbent proceeded principally

Table 3
Isotherm constants for the adsorption of copper, nickel and zinc on ACMO.

Metal	T (K)	Langmuir constants			Freundlich constants			D–R constants				Temkin constants		
		X_m (mg g^{-1})	b (L mg^{-1})	R^2	n	K (mg g^{-1})	R^2	K	q_m (mg g^{-1})	R^2	E_s (kJ mol^{-1})	B	A (L g^{-1})	R^2
Copper	293	11.1359	0.1997	0.9992	2.7196	2.9122	0.9770	0.9427	8.5943	0.9046	0.7283	1.1579	3.5359	0.9969
	303	11.5340	0.2166	0.9979	2.8257	3.1963	0.9851	0.7809	8.8693	0.8893	0.8002	1.1198	2.7984	0.9989
	313	12.3609	0.2195	0.9940	2.8474	3.4674	0.9950	0.6390	9.2766	0.8590	0.8846	1.0368	2.5436	0.9942
	323	13.1234	0.2389	0.9902	2.9214	3.8563	0.9976	0.4912	9.7484	0.8366	1.0089	0.9762	2.2016	0.9855
Nickel	293	19.7629	0.7377	0.9980	2.7647	7.8444	0.9324	0.1099	15.6286	0.9462	2.1330	0.7182	1.5375	0.9935
	303	19.0840	0.6165	0.9973	2.6976	7.0766	0.9110	0.1677	15.2244	0.9558	1.7267	0.6993	1.6256	0.981
	313	18.7266	0.4877	0.9956	2.5853	6.3325	0.8857	0.2775	15.1107	0.9765	1.3423	0.6651	1.7755	0.9683
	323	18.1159	0.3943	0.9935	2.4777	5.5823	0.8528	0.4672	14.8396	0.9891	1.0345	0.6398	1.9986	0.9473
Zinc	293	17.8571	0.1725	0.9737	2.2528	3.7708	0.9996	0.4600	11.4834	0.8197	1.0426	0.7317	4.1141	0.9667
	303	17.6678	0.1430	0.9528	2.2143	3.4076	0.9960	0.5834	10.9430	0.7955	0.9258	0.7218	6.3031	0.9439
	313	16.5838	0.1310	0.9637	2.1959	3.0569	0.9959	0.7968	10.3584	0.8010	0.7922	0.7308	11.7366	0.9540
	323	15.625	0.1232	0.9684	2.1711	2.7713	0.9917	1.0654	9.8789	0.8085	0.6851	0.7338	32.3729	0.9561

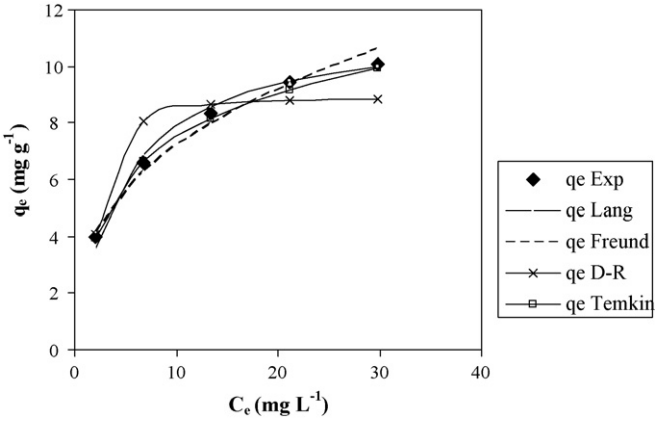

Fig. 8. Adsorption isotherm for Cu, experimental and predicted by Langmuir, Freundlich, D–R and Temkin models at 303 K, carbon dosage 0.2 g (100 mL)$^{-1}$, pH 6, time 4 h.

by physical adsorption. From the E_s value, the multilayer sorption behaviour of metals was also proven by the D–R isotherm.

The comparison of the experimental values with the values of q_e for all the metals obtained by the above models is shown in Figs. 8–10. As seen from the figure, Langmuir, Freundlich and Temkin isotherms were well fitted with the experimental data for Cu, Langmuir model for Ni and Langmuir and Freundlich models for Zn. It was also observed that the monolayer adsorption capacity is maximum in the case of Ni to an extent of 19.08 mg g^{-1} followed by Zn (17.67 mg g^{-1}) and Cu showing the least adsorption capacity of 11.53 mg g^{-1} (at 303 K). The results obtained from this study indicate that the ACMO is a suitable adsorbent for all the metals. Table 4 gives a comparison of the adsorption capacity of Cu, Ni and Zn on different adsorbents taken from the literature.

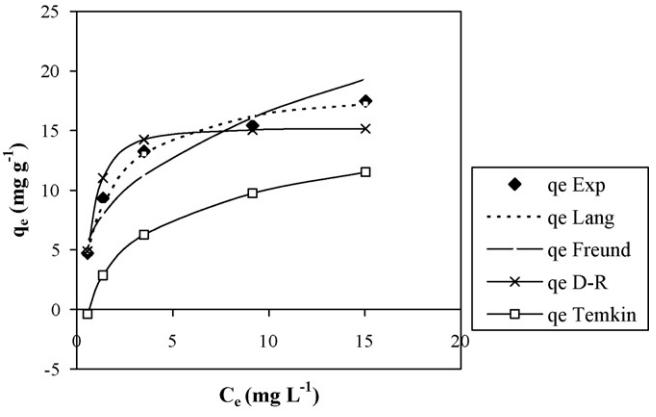

Fig. 9. Adsorption isotherm for Ni, experimental and predicted by Langmuir, Freundlich, D–R and Temkin models at 303 K, carbon dosage 0.2 g (100 mL)$^{-1}$, pH 6, time 4 h.

3.4. Kinetic studies

The kinetic studies describe the solute uptake rate, which in turn governs residence time of adsorption process. It is one of the important characteristics in defining the efficiency. In the present study, the kinetics of the metal ion removal was carried out to understand the behaviour of ACMO. The kinetics of Cu, Ni and Zn on ACMO were analyzed by pseudo-first-order and pseudo-second-order model at different temperatures.

3.4.1. Pseudo-first-order model

The pseudo-first-order Lagergren model is expressed as [44],

$$\ln(q_e - q_t) = \ln(q_e) - K_1 t \quad (12)$$

where q_e and q_t refer to the amount of metal ion adsorbed per unit weight of adsorbent (mg g^{-1}) at equilibrium and at any time t (min). The value of q_e and first-order adsorption rate constant K_1 (min^{-1}) can be obtained from the plot of $\ln(q_e - q_t)$ versus t.

3.4.2. Pseudo-second-order model

The pseudo-second-order model is based on the assumption that adsorption follows a second-order mechanism. So, the rate of occupation of adsorption sites is proportional to the square of the number of unoccupied sites. It can be given as [45],

$$\frac{t}{q_t} = \left[\frac{1}{K_2 q_e^2} + \frac{t}{q_e}\right] \quad (13)$$

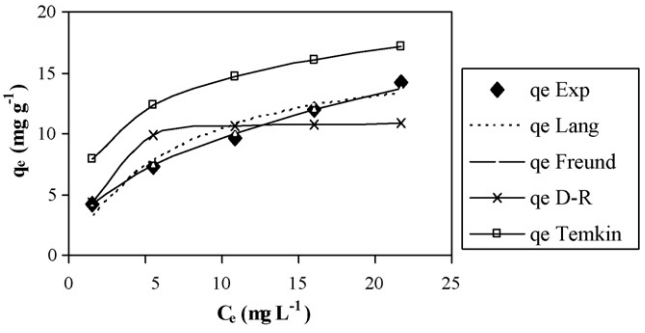

Fig. 10. Adsorption isotherm for Zn, experimental and predicted by Langmuir, Freundlich, D–R and Temkin models at 303 K, carbon dosage 0.2 g (100 mL)$^{-1}$, pH 6, time 4 h.

Table 4
Comparison of adsorption capacity of various adsorbents for Cu, Ni and Zn.

Adsorbent	Adsorption capacity (mg g^{-1})			Reference
	Copper	Nickel	Zinc	
Rubber wood sawdust A.C.	5.729	–	–	[25]
Hazelnut husk A.C.	6.645	–	–	[51]
Activated carbon	3.56	–	–	[52]
Spent activated clay	10.9	–	–	[53]
Activated poplar sawdust	9.24	–	–	[54]
Rice hulls activated carbon	3.92	–	–	[55]
Activated carbon from sugar beet pulp (300 °C)	68.03	–	–	[56]
Activated carbon from sugar beet pulp (400 °C)	71.99	–	–	[56]
Activated carbon from sugar beet pulp (500 °C)	79.99	–	–	[56]
Carbon prepared from apricot stones	12.01	–	13.21	[57]
Carbon prepared from coconut shells	11.10	–	–	[57]
Carbon prepared from lignite coal	9.80	–	–	[57]
Carbon prepared from peanut hulls	89.29	–	–	[58]
Commercial activated carbon, India	2.74	–	–	[58]
Activated carbon	31.11	–	–	[59]
Hazelnut husk A.C. (20 °C)	–	5.757	–	[60]
Hazelnut husk A.C. (3 °C)	–	7.181	–	[60]
Hazelnut husk A.C. (40 °C)	–	10.107	–	[60]
Hazelnut husk A.C. (50 °C)	–	11.64	–	[60]
Peanut hull carbon	–	53.65	–	[61]
Granular activated carbon	–	1.49	–	[61]
Coirpith carbon	–	62.5	–	[62]
A.C. from apricot (400 °C)	–	17.04	–	[63]
A.C. from apricot (500 °C)	–	22.47	–	[63]
A.C. from apricot (600 °C)	–	19.37	–	[63]
A.C. from apricot (700 °C)	–	35.59	–	[63]
A.C. from apricot (800 °C)	–	32.36	–	[63]
A.C. from apricot (900 °C)	–	101.01	–	[63]
Acid-treated coconut shell carbon (ACSC)	–	–	45.14	[64]
Chitosan coated coconut shell carbon (CCSC)	–	–	50.93	[64]
Chitosan coated ACSC (CACSC)	–	–	60.41	[64]
Calcined phosphate	–	–	23.7	[65]
Red mud	–	–	12.59	[66]
Lignite	–	–	22.83	[67]
Peat	–	–	9.28	[68]
Blast furnace slag	–	–	17.65	[69]
ACMO	11.534	19.084	17.668	Present study

The product $K_2 q_e^2$ is the initial sorption rate. A plot of t/q_t against t at different temperatures provides second-order adsorption rate constants K_2 (g mg^{-1} min^{-1}) and q_e values from the slopes and intercepts.

The kinetic constants along with the correlation coefficients are listed in Table 5. The experimental q_e values were compared to q_e values determined by pseudo-first and second-order rate kinetic models. The Lagergren first-order rate constant K_1 and q_e determined from the model indicates that this model had failed to estimate q_e since the experimental value of q_e differs from estimated one. The best fit for the experimental data of this study was achieved by the application of pseudo-second-order kinetic equation. The coefficient of correlation for second-order kinetic model was greater than 0.9995 and the estimated value of q_e also agreed with the experimental one. Both factors suggest that the adsorption of metal ions followed the second-order kinetic model, indicating that the rate limiting step was a chemical adsorption process between metal ion and ACMO. This provides the best correlation of the data.

3.5. Adsorption mechanism

The adsorption mechanism consist of three stages: (1) transport of the adsorbate to the external surface of the adsorbent (film diffusion); (2) transport of the adsorbate within the pores of the adsorbent (intra-particle diffusion); and (3) adsorption of the adsorbate on the exterior surface of the adsorbent. Step (3) is rapid and does not represent the rate-determining step in the uptake of adsorbate. The slowest step determines the rate-controlling parameter in the adsorption process. However, the rate-controlling parameter might be distributed between intra-particle and film diffusion mechanisms.

The most commonly used technique for identifying the mechanism involved in the sorption process is by fitting the experimental data in an intra-particle diffusion plot. Previous studies [25] showed that the plot of q_t versus $t^{0.5}$ represents multi linearity, which characterizes the two or more steps involved in the sorption process. The intra particle diffusion model [46] can be given as

$$q_t = K_{id} t^{0.5} \tag{14}$$

where K_{id} is initial rate of the intra particle diffusion (mg (g min$^{0.5}$)$^{-1}$). The value of K_{id} can be obtained from the slope of the plot of q_t versus $t^{0.5}$. From Fig. 11, it was noted that the sorption process tends to be followed by two portions. The two portions in the intra-particle diffusion plot suggest that the adsorption process proceeds by surface adsorption and intra-particle diffusion. The initial curved portion of the plot indicates a boundary layer effect while the second linear portion is due to intra-particle or pore diffusion. The slope of the second linear portion of the plot has been defined as the intra-particle diffusion parameter, K_{id}. On the other hand, the intercept of the plot reflects the boundary layer effect. The larger the intercept, the greater the contribution of the surface sorption in the rate limiting step. The calculated intra-particle diffusion coefficient for Cu, Ni and Zn at different temperatures are listed in Table 6. The intra-particle diffusion rate constants were found to increase for Cu and decrease for Ni and Zn with temperature.

Kinetic data obtained in this work were analyzed by applying simplified form of Vermeulen's approximation [47] of the model of

Table 5
Kinetic constants for the adsorption of copper, nickel and zinc ions on ACMO.

Metal	T (K)	Pseudo-first-order model			Pseudo-second-order model			q_e (expt.)(mg g^{-1})
		q_e (cal) (mg g^{-1})	K_1 (min^{-1})	R^2	q_e (cal) (mg g^{-1})	K_2 (g mg^{-1} min^{-1})	R^2	
Copper	293	1.8445	0.0156	0.7160	8.0515	0.0735	0.9996	8.0766
	303	1.7688	0.0169	0.7254	8.3264	0.0848	0.9998	8.3406
	313	1.7484	0.0214	0.7907	8.6356	0.1080	0.9999	8.6310
	323	2.0245	0.0201	0.7972	9.0253	0.0776	0.9998	9.0270
Nickel	293	1.0316	0.0199	0.6234	13.3869	0.2608	1	13.4007
	303	1.0593	0.0200	0.6370	13.2450	0.2457	1	13.2537
	313	1.0114	0.0315	0.6111	12.9199	0.4992	1	12.9228
	323	1.0700	0.0190	0.5794	12.6103	0.2898	1	12.6287
Zinc	293	2.3625	0.0184	0.7843	10.2669	0.0570	0.9996	10.2708
	303	1.9923	0.0271	0.8760	9.6154	0.0957	0.9999	9.5847
	313	1.5199	0.0171	0.6673	9.0580	0.1106	0.9999	9.0772
	323	1.8938	0.0239	0.8469	8.6505	0.0986	0.9999	8.6354

Table 6
Intra-particle diffusion rate parameter and effective diffusion coefficient at different temperatures.

T (K)	Copper		Nickel		Zinc	
	$K_{id} \times 10^2$ (mg g^{-1} min$^{-0.5}$)	$D_e \times 10^{12}$ (m^2 s^{-1})	$K_{id} \times 10^2$ (mg g^{-1} min$^{-0.5}$)	$D_e \times 10^{12}$ (m^2 s^{-1})	$K_{id} \times 10^2$ (mg g^{-1} min$^{-0.5}$)	$D_e \times 10^{12}$ (m^2 s^{-1})
293	8.48	1.9578	3.96	2.9992	11.48	4.7209
303	8.63	2.1383	3.76	2.6659	9.52	3.5684
313	8.84	2.7631	2.37	2.5687	8.39	3.2074
323	8.94	2.7909	2.28	2.3882	7.16	3.1102

Boyd et al. [48], for the calculation of effective particle diffusivity of metal ions onto ACMO using following equation,

$$F(t) = \left[1 - \exp\left(\frac{-\pi^2 D_e t}{{R_a}^2}\right)\right]^{1/2} \quad (15)$$

$$F(t) = \frac{q_t}{q_e},$$

where $F(t)$ is the fractional attainment of equilibrium at time t, D_e (m^2 s^{-1}) is the effective diffusion coefficient, R_a(m) is the radius of spherical adsorbent particles.

The slope of the plot of $\ln[1/(1 - F^2(t))]$ versus t gives D_e. Table 6 presents the values of effective diffusion coefficient (D_e) of Cu, Ni and Zn at different temperatures. Average values of D_e are found to be in the order of 10^{-12} m^2 s^{-1} for the adsorption of Cu, Ni and Zn ions onto ACMO. Diffusion coefficient values for all the metal ions follow the same trend. Chen et al. [49] have reported a D_e value of 2×10^{-12} m^2 s^{-1} for the Cu adsorption onto granular activated carbon. Srivastava et al. [50] have reported D_e values of 5.780×10^{-13} and 6.848×10^{-13} m^2 s^{-1}, respectively, for the adsorption of Ni and Zn ions onto rice husk ash. The above values are quite comparable to the values obtained in the present study. The pores have different sizes along their lengths and the ACMO has a wide pore size distribution. The adsorbent–adsorbate and adsorbate–adsorbate interactions have their impact on the diffusion process and affect the value of D_e. The properties of the adsorbents–the pore size along length of the pore, orientation, electronic field and the interaction of the adsorbate–physicochemical attraction–vander Waals forces, etc., size of the adsorbents, surface diffusion characteristics and adsorption mechanism, all affect the diffusion. Although diffusion coefficient values are low, they are high enough to cause adsorbate transport from bulk to solid phase. For the present systems, the values of D_e shown in Table 6, fall well within the values reported in literature, specifically for chemisorption systems (10^{-9} to 10^{-17} m^2 s^{-1}).

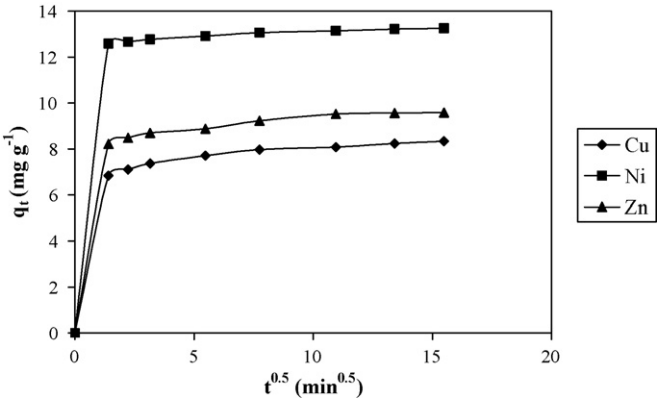

Fig. 11. Intra-particle diffusion plot for the adsorption of Cu, Ni and Zn onto ACMO at 303 K, initial metal ion concentration 30 mg L^{-1}, carbon dosage 0.2 g (100 mL)$^{-1}$, pH 6.

3.6. Desorption characterization

3.6.1. Recovery of adsorbed metal from ACMO

To investigate the possibility of repeated use of the adsorbent, desorption experiments were conducted under batch experimental conditions and desorption efficiencies were compared in Fig. 12. The use of demineralised water showed insignificant metal desorption capacity (<1%). The use of Na_2CO_3, $NaHCO_3$, and NH_4Cl solutions resulted in only limited amount of metal desorption (<25%). Acetic acid showed a desorption efficiency of about 45.32% (copper), 47.12% (nickel) and 49.56% (zinc). On the other hand, acids, HCl, HNO_3 and H_2SO_4, resulted in high recovery efficiencies of about 95.78%, 82.11% and 99.81% for copper, 96.31%, 85.03% and 99.92% for nickel and 95.71%, 86.72% and 99.03% for zinc respectively. In addition, complexing agent EDTA also resulted in high recovery efficiency of 99% for all the three metals. The low desorption efficiencies of Na_2CO_3, $NaHCO_3$, and NH_4Cl can be attributed to the fact that the metal ions are reacting much faster with acids than base. EDTA had similar regeneration efficiency to that of H_2SO_4. This can be attributed to its strong complexing ability to metal ions. However, it has the disadvantage of high cost and it is also difficult to recover the metal ions from EDTA solution as the stability

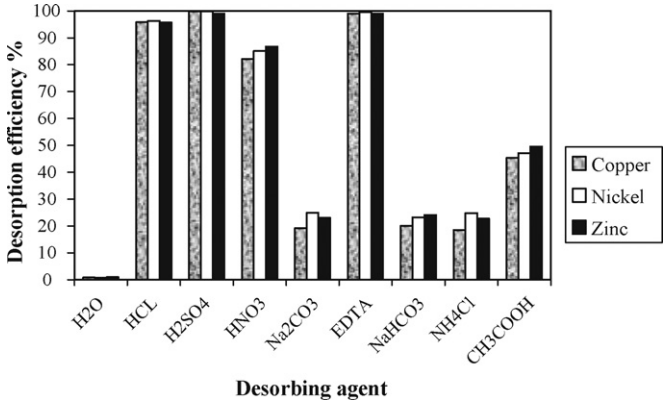

Fig. 12. Desorption efficiencies of metal ions from ACMO by using different desorbing agents (concentration of desorbing agents: 0.1 M, ACMO: 0.2 g (100 mL)$^{-1}$.

of metal–EDTA complex is very high. Overall, H_2SO_4 was selected as the optimal eluting agent for the system studied. Adsorption experiments were conducted and adsorbents loaded with metals were desorbed using H_2SO_4 solutions of different concentrations. The amount of metal ions released back into the solution was then determined and expressed as a desorption efficiency as shown in Fig. 13. The results show that increasing the concentrations of H_2SO_4 increased the desorption efficiency, however, an optimum was observed at 0.1 M concentration beyond which the efficiency of desorption remained a constant. Therefore, the concentration of 0.1 M was used for elution in further studies. This is further evidence that ion-exchange was the mechanism involved in the adsorption process.

3.6.2. Adsorption–desorption cycles

Reusability of an adsorbent is of crucial importance in industrial practice for metal removal from wastewater. In order to show the reusability of ACMO, adsorption–desorption cycle of copper, nickel and zinc was repeated several times using the same adsorbent. The metal ions adsorbed onto ACMO were desorbed with 0.1 M H_2SO_4 in batch system. Approximately 98% of the adsorbed metal ions were desorbed from ACMO. It was observed that the Cu uptake for cycles 2–6 (Fig. 14), Ni uptake for cycles 2–7 (Fig. 15) and Zn uptake for cycles 2–7(Fig. 16), although slightly lower than that for cycle 1, were reasonably consistent irrespective of the number of cycles. The total decrease in adsorption efficiency of ACMO was about 9.15% for Cu (after six cycles), 10.3% for Ni (after seven cycles) and 11.78% for Zn (after seven cycles) which shows that ACMO has good potential to adsorb metal ions from aqueous solution.

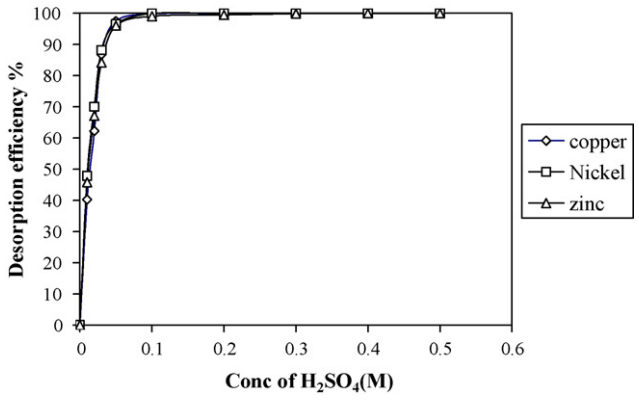

Fig. 13. Effect of H_2SO_4 concentration on the desorption of Cu, Ni and Zn from ACMO.

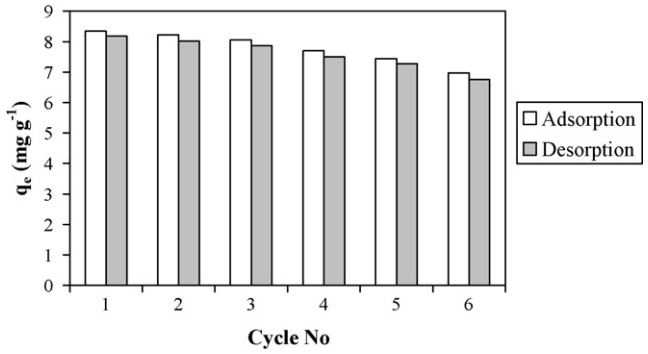

Fig. 14. Adsorption–desorption of copper by ACMO in six consecutive cycles.

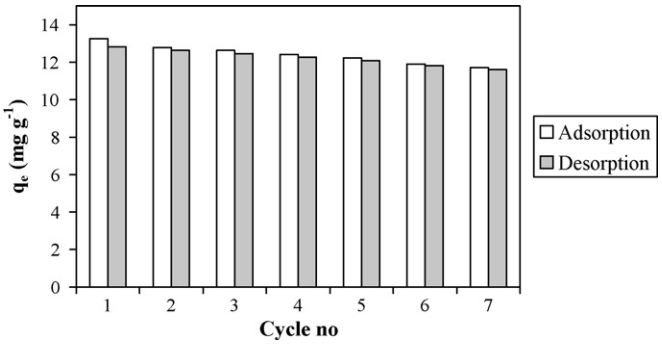

Fig. 15. Adsorption–desorption of nickel by ACMO in seven consecutive cycles.

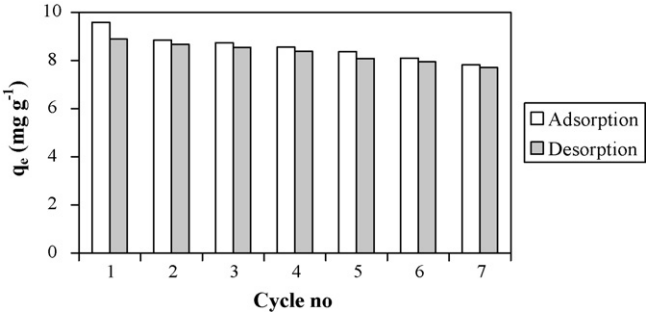

Fig. 16. Adsorption–desorption of zinc by ACMO in seven consecutive cycles.

4. Conclusion

Moringa oleifera wood precursors were found to be a good raw material for developing activated carbon. The activated carbon produced has high surface area. ACMO was found to be a promising adsorbent for the removal of Cu, Ni and Zn from aqueous solution. The surface morphology and functional groups involved in all the adsorbents were determined by analyzing through SEM and FT IR. Adsorption capacity of ACMO was highly dependent on the initial concentrations of metal ion, carbon dosage, contact time, pH and temperature. The optimum pH was found to be 6. The adsorption process is spontaneous, endothermic for Cu, and exothermic for Ni and Zn. Langmuir, Freundlich, Temkin and Dubinin Radeshkevich isotherm models were employed to describe the metal ion adsorption at different temperatures. Langmuir, Freundlich and Temkin model fits the experimental data better for Cu, Langmuir model for Ni and Langmuir and Freundlich models for Zn. ACMO showed highest adsorption capacity for removal of Ni followed by Zn and Cu. Among the kinetic models tested, the adsorption kinetics was best described by the pseudo-second-order equation for all the metal

ions. The adsorption process was found to be controlled by both film diffusion and intra-particle diffusion. ACMO could be regenerated and reused for six adsorption and desorption cycles for Cu, seven adsorption–desorption cycles for Ni and Zn with a little decrease in the metal uptake capacity of the carbon. The data from the present study showed that the MO is inexpensive, indigenous, easily available material and ACMO has good potential in treating metal laden industrial effluents.

References

[1] R.E. Clement, G.A. Eiceman, C.J. Koester, Environmental analysis, Anal. Chem. 67 (1995) 221R–255R.
[2] P. MacCarthy, R.W. Klusman, S.W. Cowling, J.A. Rice, Water analysis, Anal. Chem. 67 (1995) 525R–582R.
[3] D.G. Barceloux, Copper, J. Toxicol. Clin. Toxicol. 37 (1999) 217–230.
[4] D.G. Barceloux, Nickel, J. Toxicol. Clin. Toxicol. 37 (1999) 239–258.
[5] D.C. Burrell, Atomic Spectrometric Analysis of Heavy Metal Pollutants in Water, Ann Arbor Science Publishers, Ann Arbor, Michigan, 1974, pp. 19–45.
[6] E. Berman, Toxic Metals and their Analysis, Heyden, London, 1980.
[7] WHO's Guidelines for Drinking-water Quality, set up in Geneva, 1993.
[8] N. Meunier, P. Drogui, C. Montane, R. Hausler, G. Mercier, J.F. Blais, Comparison between electrocoagulation and chemical precipitation for metals removal from acidic soil leachate, J. Hazard. Mater. 137 (2006) 581–590.
[9] T.A. Kurniawan, G.Y.S. Chan, W.H. Lo, S. Babel, Physico-chemical treatment techniques for wastewater laden with heavy metals, Chem. Eng. J. 118 (2006) 83–98.
[10] E.L. Cochrane, S. Lu, S.W. Gibb, I. Villaescusa, A comparison of low-cost biosorbents and commercial sorbents for the removal of copper from aqueous media, J. Hazard. Mater. 137 (2006) 198–206.
[11] S.K. Srivastava, R. Tyagi, N. Pant, Adsorption of heavy metal ions on carbonaceous material developed from the waste slurry generated in local fertilizer plants, Water Res. 23 (1989) 1161–1165.
[12] P. Galiatsatou, M. Metaxas, R.V. Kasselouri, Adsorption of zinc by activated carbon prepared from solvent extracted olive pulp, J. Hazard. Mater. B91 (2002) 187–203.
[13] S.E. Bailey, T.J. Olin, R.M. Bricka, D.D. Adrian, A review of potentially low-cost sorbents for heavy metals, Water Res. 33 (1999) 2469–2479.
[14] S. Sirianuntapiboon, T. Hongsrisuwan, Removal of Zn^{2+} and Cu^{2+} by a sequencing batch reactor (SBR) system, Bioresour. Technol. 98 (2007) 808–818.
[15] J.T. Matheickal, Q. Yu, Biosorption of lead(II) and copper(II) from aqueous solutions by pre-treated biomass of Australian marine algae, Bioresour. Technol. 69 (1999) 223–229.
[16] R.C. Bansal, J.B. Donnet, F. Stoeckli, Active Carbon, Marcel Dekker, New York, 1988.
[17] F. Rodrıguez-Reinoso, M. Molina-Sabio, Activated carbons from lignocellulosic materials by chemical and/or physical activation: an overview, Carbon 30 (1992) 1111–1118.
[18] T. Wigmans, Industrial aspects of production and use of activated carbon, Carbon 27 (1989) 13–22.
[19] M. Jaytogen, M. Thwaites, J. Stencel, B. McEnaney, F. Derbyshire, Adsorbent carbon synthesis from coals by phosphoric acid activation, Carbon 30 (1992) 1089–1096.
[20] A.M. Warhurst, G.L. McConnachie, S.J.T. Pollard, Characterisation and applications of activated carbon produced from *Moringa oleifera* seed husks by single-step steam pyrolysis, Water Res. 31 (1997) 759–766.
[21] A.M. Warhurst, G.L. McConnachie, S.J.T. Pollard, The production of activated carbon for water treatment in Malawi from the waste seed husks of *Moringa oleifera*, Water Sci. Tech. 34 (1996) 177–184.
[22] H.N. Bhatti, B. Mumtaz, M.A. Hanif, R. Nadeem, Removal of Zn(II) ions from aqueous solution using *Moringa oleifera* Lam. (horseradish tree) biomass, Proc. Biochem. 42 (2007) 547–553.
[23] D.H. Kumar Reddy, K. Seshaiah, A.V.R. Reddy, M. Madhava Rao, M.C. Wang, Biosorption of Pb^{2+} from aqueous solutions by *Moringa oleifera* bark: Equilibrium and kinetic studies, J. Hazard. Mater. 174 (2010) 831–838.
[24] P. Sharma, P. Kumari, M.M. Srivastava, S. Srivastava, Removal of cadmium from aqueous system by shelled *Moringa oleifera* Lam. seed powder, Bioresour. Technol. 97 (2006) 299–305.
[25] M. Helen Kalavathy, T. Karthikeyan, S. Rajgopal, L.R. Miranda, Kinetic and isotherm studies of Cu(II) adsorption onto H_3PO_4– activated rubber wood sawdust, J. Colloid Interface Sci. 292 (2005) 354–362.
[26] M.S. Onyango, Y. Kojima, O. Aoyi, E.C. Bernardo, H. Matsuda, Adsorption Equilibrium modeling and solution chemistry dependence of fluoride removal from water by trivalent cation-exchange zeolite F-9, J. Colloid Interface Sci. 279 (2004) 341–350.
[27] ASTM D 4607-86 Philadelphia, PA: ASTM Committee on Standards, 1986.
[28] G.H. Jeffery, J. Bassett, J. Mendham, R.C. Denny, Vogel's Text Book of Quantitative Chemical Analysis, 5th edition, John Wiley and sons, New York, 1996.
[29] N. Manivasakam, Industrial Effluents Origin, Characteristics. Effects Analysis and Treatment, Sakthi Publication, Coimbatore, India, 1987.
[30] M.S. Nomanbhay, K. Palanisamy, Removal of Heavy metal from industrial waste using chitosan coated oil palm shell charcoal, Electron. J. Biotechnol. 8 (2005) 43–53.
[31] I.D. Mall, V.C. Srivastava, N.K. Agarwal, I.M. Mishra, Removal of congo red from aqueous solution by bagasse fly ash and activated carbon: Kinetic study and equilibrium isotherm analyses, Chemosphere 61 (2005) 492–501.
[32] B.M.W.P.K. Amarasinghe, R.A. Williams, Tea waste as a low cost adsorbent for the removal of Cu and Pb from wastewater, Chem. Eng. J. 132 (2007) 299–309.
[33] G. McKay, M.S. Otterburn, A.G. Sweeney, The removal of colour from effluents using various adsorbents-III silica rate process, Water Res. 14 (1980) 15–20.
[34] C. Namasivayam, R.T. Yamuna, Adsorption of chromium(VI) by a low cost adsorbent: Biogas residual slurry, Chemosphere 30 (1993) 561–578.
[35] Y.S. Ho, J.F. Porter, G. McKay, Equilibrium isotherm studies for the sorption of divalent metal ions onto peat: copper, nickel and lead single component systems, Water Air Soil Pollut. 141 (2002) 1–33.
[36] Y. Orhan, H. Bugukgunor, The removal of heavy metals by using agricultural wastes, Water Sci. Technol. 28 (1993) 247–255.
[37] I. Langmuir, The adsorption of gases on plane surfaces of glass, mica and platinum, J. Am. Chem. Soc. 40 (1918) 1361–1403.
[38] H.M.F. Freundlich, Over the adsorption in solution, Z. Phys. Chem. 57A (1906) 385–470.
[39] M.J. Temkin, V. Pyzhev, Kinetics of ammonia synthesis on promoted iron catalysts, Acta Physiochim. URSS 12 (1940) 327–356.
[40] M.M. Dubinin, The potential theory of adsorption of gases and vapors for adsorbents with energetically non-uniform surface, Chem. Rev. 60 (1960) 235–266.
[41] W. Rieman, H. Walton, Ion Exchange in Analytical Chemistry, International Series of Monographs in Analytical Chemistry, vol. 38, Pergamon Press, Oxford, 1970.
[42] M.S. Onyango, Y. Kojima, A. Kumar, D. Kuchar, M. Kubota, H. Matsuda, Uptake of fluoride by Al^{3+} pretreated low-silica synthetic zeolites: adsorption equilibrium and rate studies, Sep. Sci. Technol. 41 (2006) 683–704.
[43] A. Agrawal, K.K. Sahu, B.D. Pandey, Removal of zinc from aqueous solutions using sea nodule residue, Colloids Surf. A: Physicochem. Eng. Asp. 237 (2004) 133–140.
[44] S. Lagergren, Zur theorie der sogenannten adsorption gelöster stoffe, Kungliga Svenska Vetenskapsakademiens. Handlingar 24 (1898) 1–39.
[45] T.S. Ho, G. McKay, The Kinetics of sorption of basic dyes from aqueous solution by sphagnum moss peat, Can. J. Chem. Eng. 76 (1998) 822–827.
[46] W.J. Weber, J.C. Morris, Kinetics of adsorption on carbon from solution, J. Sanit. Eng. Div. Am. Soc. Civ. Eng. 89 (1963) 31–60.
[47] T. Vermeulen, Theory of irreversible and constant-pattern solid diffusion, Ind. Eng. Chem. 45 (1953) 1664–1670.
[48] G.E. Boyd, A.W. Adamson, L.S. Meyers, The exchange adsorption of ions from solution from organic zeolites. II. Kinetics, J. Am. Chem. Soc. 69 (1947) 2836–2848.
[49] B. Chen, C.M. Hui, G. Mckay, Film-pore diffusion modelling for the sorption of metal ions from aqueous effluents onto peat, Water Res. 35 (2001) 3345–3356.
[50] V.C. Srivastava, I.D. Mall, I.M. Mishra, Characterization of mesoporous rice husk ash (RHA) and adsorption kinetics of metal ions from aqueous solution onto RHA, J. Hazard. Mater. B134 (2006) 257–267.
[51] M. Imamoglu, O. Tekir, Removal of copper (II) and lead (II) ions from aqueous solutions by adsorption on activated carbon from a new precursor hazelnut husks, Desalination 228 (2008) 108–113.
[52] M. Machida, M. Aikawa, H. Tatsumoto, Prediction of simultaneous adsorption of Cu(II) and Pb(II) onto activated carbon by conventional Langmuir type equations, J. Hazard. Mater. B120 (2005) 271–275.
[53] C.H. Weng, C.Z. Tsai, S.H. Chu, Y.C. Sharma, Adsorption characteristics of copper(II) onto spent activated clay, Sep. Purif. Technol. 54 (2007) 187–197.
[54] F.N. Acar, Z. Eren, Removal of Cu(II) ions by activated poplar sawdust (Samsun Clone) from aqueous solutions, J. Hazard. Mater. 137 (2006) 909–914.
[55] M. Teker, M. Imamoglu, O. Saltabas, Adsorption of copper and cadmium ions by activated carbon from rice hulls, Turkish J. Chem. 23 (1999) 185–191.
[56] A. Ozer, F. Tumen, Cd(II) adsorption from aqueous solution by activated carbon from sugar beet pulp impregnated with phosphoric acid, Fresen. Environ. Bull. 12 (2003) 1050–1058.
[57] T.K. Budinova, K.M. Gergova, N.V. Petrov, V.N. Minkova, Removal of metal ions from aqueous solution by activated carbons obtained from different raw materials, J. Chem. Technol. Biotechnol. 60 (1994) 177–182.
[58] K. Periasamy, C. Namasivayam, Process development for removal and recovery of cadmium from wastewater by a low-cost adsorbent: adsorption rates and equilibrium studies, Ind. Eng. Chem. Res. 33 (1994) 317–320.
[59] D. Mohan, K.P. Singh, Single-and multi-component adsorption of cadmium and zinc using activated carbon derived from bagasse—an agricultural waste, Water Res. 36 (2002) 2304–2318.
[60] E. Demirbas, M. Kobya, S. Oncel, S. Sencan, Removal of Ni(II) from aqueous solution by adsorption onto hazelnut shell activated carbon: equilibrium studies, Bioresour. Technol. 84 (2002) 291–293.
[61] K. Periasamy, C. Namasivayam, Removal of nickel (II) from aqueous solution wastewater using an agricultural waste: peanut hulls, Waste Manage. 15 (1995) 63–68.
[62] K. Kadirvelu, K. Thamaraiselvi, C. Namasivayam, Adsorption of nickel(II) from aqueous solution onto activated carbon prepared from coirpith, Sep. Purif. Technol. 24 (2001) 497–505.
[63] S. Erdogan, Y. Onal, C. Akmil-Basar, S. Bilmez-Erdemoglu, C. Sarıcı-Ozdemir, E. Koseoglu, G. Icduygu, Optimization of nickel adsorption from aqueous solution by using activated carbon prepared from waste apricot by chemical activation, Appl. Surf. Sci. 252 (2005) 1324–1331.

[64] O.S. Amuda, A.A. Giwa, I.A. Bello, Removal of heavy metal from industrial wastewater using modified activated coconut shell carbon, Biochem. Eng. J. 36 (2007) 174–181.
[65] A. Aklil, M. Mouflih, S. Sebti, Removal of heavy metal ions from water by using calcined phosphate as a new adsorbent, J. Hazard. Mater. A112 (2004) 183–190.
[66] E. Lopez, B. Soto, M. Arias, A. Nunez, D. Rubinos, M.T. Barral, Adsorbent properties of red mud and its use for wastewater treatment, Water Res. 32 (1998) 1314–1322.
[67] S.J. Allen, P. Brown, Isotherm analysis for single component and multi-component metal sorption onto lignite, J. Chem. Technol. Biotechnol. 62 (1995) 17–24.
[68] G. McKay, B. Vong, J.F. Porter, Isotherm studies for the sorption of metal ions onto peat, Adsorpt. Sci. Technol. 16 (1998) 51–66.
[69] S.K. Srivastava, V.K. Gupta, D. Mohan, Design parameters for fixed bed reactors of activated carbon developed from fertilizer waste for the removal of some heavy metal ions, Waste Manage. 17 (1997) 517–522.